

I-section flange compactness under minor axis flexure

M. Aktas[†]

Department of Civil Engineering, Sakarya University, Sakarya, Turkey

C. J. Earls[‡]

Department of Civil & Environmental Engineering, University of Pittsburgh, Pittsburgh, Pennsylvania, 15261, USA

(Received July 5, 2005, Accepted January 20, 2006)

Abstract. The present paper hopes to elucidate the problem of determining if a given I-shaped cross-section is properly proportioned to accommodate sufficient plastic hinge rotation capacity to facilitate the redistribution of moments in a structural system as needed to accommodate the formation of a collapse mechanism. It might be tempting to believe that application of the limiting flange plate slenderness value for the case of major axis flexure are applicable in this case; since the pervasive belief is that this approach ought to be conservative. However, the present research study indicates that this is not the case and thus more sophisticated analysis techniques are required to better understand this case.

Keywords: compactness; minor axis bending; rotation capacity; finite element modelling; imperfection; weak axis bending.

1. Introduction

The case of minor axis flexure in I-shaped cross-sections arises frequently in the consideration of bi-axial beam bending associated with perimeter spandrel members in exterior framing lines, as well as in the general case of a beam-column. In these instances, it may be desirable to employ cross-sections whose proportions are such that sufficient structural ductility is available in the member in order that system-wide moment redistribution may be achieved. Scenarios requiring this capacity to redistribute forces frequently arise in seismic design and other applications that require structural robustness against natural and man-made hazards.

1.1. Basis for current cross-sectional compactness limits for unstiffened elements

The goal of the US specification in its prescription of so-called compactness criteria (AISC 1999) is to identify plate slenderness limits, λ_p , for cross-sectional plate components such that an overall flexural

[†]Assistant Professor, Corresponding author, E-mail: muharremaktas@gmail.com

[‡]Associate Professor & William Kepler Whiteford Faculty Fellow

cross-section will be able to accommodate sufficient plastic hinge rotation to support system-wide moment redistribution as required for the development of a global collapse mechanism. In pursuit of this condition, compactness limits have historically been formulated to loosely accommodate strains approaching strain hardening values within an individual plate component prior to the attenuation of post-buckling strength due to effects of material nonlinearity.

As a point of departure for the work reported on herein, it is useful to consider the basis by which the current US Specification (AISC 1999) addresses plate compactness within the context of an unstiffened element; flanges in I-shaped cross-sections under uniform flexural compression. In this case, the question of how to address the uncertainty with regard to the nature of rotational edge restraint provided at the plate boundary associated with the flange-web junction is addressed through consideration of the work carried out by Haaijer and Thurlimann (1957). Haaijer and Thurlimann discovered that unstiffened plates exhibit the onset of strain hardening at slenderness values, λ_c , of approximately 0.46 irrespective of whether the supported edge is fixed or pinned. In this discussion, slenderness is defined as

$$\lambda_c = \sqrt{\frac{F_y}{F_{cr}}} \quad (1)$$

where classical elastic plate buckling theory provides that

$$F_{cr} = k \frac{\pi^2 E}{12(1 - \nu^2) \left(\frac{b}{t}\right)^2} \quad (2)$$

in which “ E ” and “ ν ” are the usual elastic material constants and “ b ” and “ t ” are the plate width and thickness quantities, respectively. The term “ k ” is the plate buckling coefficient which depends on the plate aspect ratio, edge support conditions, and stress distribution along the loaded edge. In the case of an I-shaped cross-sectional flange, the two extremes that “ k ” can assume are: 0.425 for the case of a supported edge that is pinned; and 1.277 for the case of a rotationally fixed supported edge. If we set Eq. (2) equal to the yield stress, F_y in psi, and solve for the width-to-thickness ratio (b/t) we obtain Eq. (3).

$$\frac{b}{t} = 162 \sqrt{\frac{k}{F_y}} \quad (3)$$

As mentioned previously, Haaijer and Thurlimann observed that unstiffened plate components under the action of a uniform edge compression achieve strain hardening response at slenderness values, λ_c , of 0.46 and thus we may use Eq. (3) to identify a plate slenderness limit for the attainment of strain hardening response as

$$\frac{b}{t} = 162 \lambda_c \sqrt{\frac{k}{F_y}} = 74.5 \sqrt{\frac{k}{F_y}} \quad (4)$$

The only question remaining regards what value to assume for the plate buckling coefficient, “ k ”. It has been standard practice for AISC (1999) to employ elastic plate buckling coefficients as a guide in the development of actual design specification equations, and as such we may consider that the two extreme values for the present case of an I-section flange: 0.425 and 1.277 for the pinned and fixed cases, respectively. If we, somewhat arbitrarily, consider one third of the difference between

these two values and add this result to the smaller of the two we obtain a “ k ” of 0.71 which can be applied to Eq. (4) so that we arrive at a limiting plate slenderness value for the onset of strain-hardening of

$$\frac{b}{t} = \frac{63}{\sqrt{F_y}} \approx \frac{65}{\sqrt{F_y}} = 0.38 \sqrt{\frac{E}{F_y}} \quad (5)$$

It is noted that Eq. (5) represents the current compactness limit, λ_p , presented in the current AISC LRFD specification (1999) in Table B5.1; for the case of an I-section flange under the action of uniform flexural compression.

We may employ a similar approach to the foregoing when developing a compactness limit for the case of flanges in I-sections subjected to flexural compression due to minor axis bending; if we assume that Haaijer and Thurlimann’s results concerning the invariance of λ_c with the degree of rotational restraint present at the supported edge in a uniformly compressed unstiffened element holds for the case of non-uniform compression. Non-uniform compression stresses would be expected along the loaded plate edge in flange outstands subjected to flexural compression (as depicted in Fig. 1). While Haaijer and Thurlimann did consider the case of non-uniform compressive stresses within a plate component, their investigation centered on the case of a stiffened element; consistent with the web of an I-shaped cross-section subjected to major axis flexure. Proceeding with the assumption that the invariance in λ_c holds for the unstiffened case of a flange outstand in flexural compression due to minor axis flexure in an I-shaped cross-section, we may reuse Eq. (4) as the basic requirement for the attainment of strain hardening in a non-uniformly compressed plate component. What is now left to do in the development of a compactness limit for flange outstands in non-uniform flexural compression is to identify a suitable plate buckling coefficient “ k ”. Guidance on the selection of an appropriate “ k ” value is obtained using the tabulated cases presented by Galambos (1998). It may be assumed that the flange outstand experiences compressive stress only (i.e., it is assumed that the neutral axis is at the flange-web junction). Two extreme values for “ k ” in this case may then be identified: 0.57 for a pinned supported edge and 1.61 for a rotationally restrained supported edge. Proceeding as in the case of an I-shaped

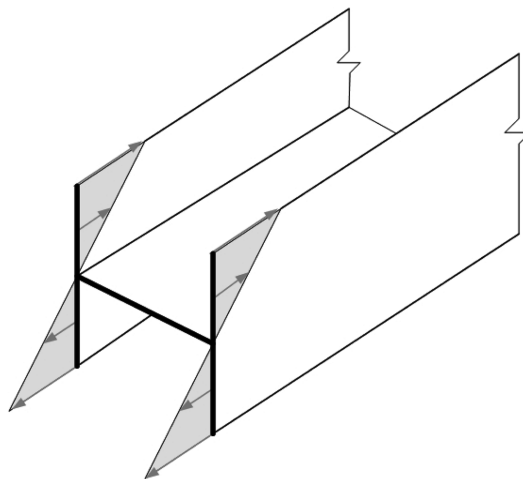


Fig. 1 Minor axis flexural normal stress distribution

beam flange outstand subjected to normal stress under major axis flexure, we may add one third of the difference between the “ k ” values of these two extremes to the smaller of the two to arrive at $k = 0.92$. We may then employ this value in Eq. (4) to arrive at a limiting plate slenderness value of

$$\frac{b}{t} = \frac{71}{\sqrt{F_y}} \approx 0.42 \sqrt{\frac{E}{F_y}} \quad (6)$$

The limits obtained from Eq. (6) can be compared with results obtained from a finite element parametric study considering flange outstands having various parametric combinations of: cross-sectional aspect ratio (B_f/d); unbraced length-to-cross-sectional depth ratio (L_b/b_f); web slenderness ratio (h/t_w); flange slenderness ratio ($B_f/2t_f$), and steel yield strength. The plate dimensional quantities indicated are explained in the nomenclature section of the present paper.

2. Finite element modeling approach

Nonlinear finite element modeling is at the heart of the research work reported on in the current paper. Given the reliance of the present work on this analytical method, it is important to clearly state the modeling approaches used, software packages employed, and any assumptions made during the construction of the finite element analogs for the I-shaped cross-sections under investigation. In addition, verification of the modeling techniques against full-scale experimental testing can be of great value. The following sub-sections endeavor to meet the above requirements and lead to a clear understanding of the approach, and subsequent limitations, of the present work.

2.1. Background

The commercial multipurpose finite element software package ABAQUS version 6.3 is employed in this research. Both nonlinear geometric and material influences as considered in all modeling. The incremental solution strategy employed in this work is the modified Riks-Wempner method (ABAQUS 2003) since this technique permits limit points on the equilibrium path to be negotiated. The ability to

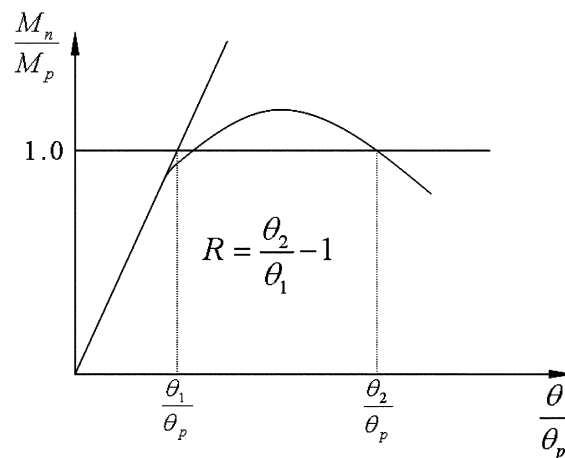


Fig. 2 Definition of rotation capacity

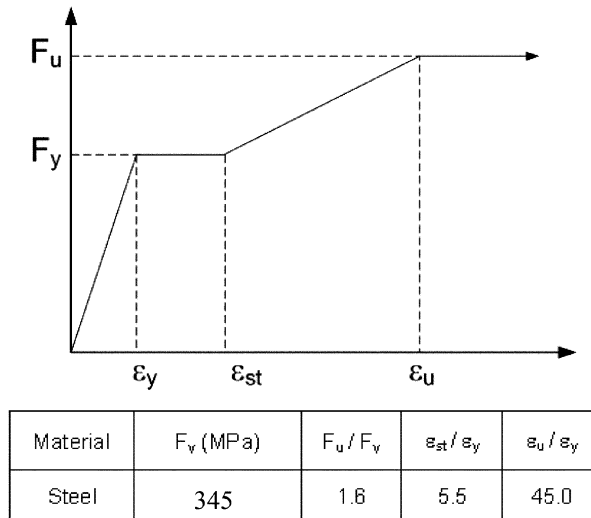


Fig. 3 Representative idealized material model used in finite element modeling

accurately negotiate such limit points is a prerequisite for any compactness study since unloading response is at the heart of the currently accepted measure for flexural ductility: rotation capacity, R . The definition for rotation capacity adopted in the present discussion is that presented by ASCE (1971): $R = \{(\theta_2/\theta_1 - 1)\}$, where θ_2 is the rotation when the moment capacity drops below M_p on the unloading branch of the M_n/M_p versus θ/θ_p plot, and θ_1 is the theoretical rotation at which the full plastic capacity is achieved based on elastic beam stiffness. This ductility response measure is described graphically in Fig. 2. It is currently assumed that $R = 3$ is an adequate level of structural ductility for the non-seismic design of steel building components (AISC 1999) and thus current compactness provisions are formulated with this measure in mind. Material nonlinearity is modeled using ABAQUS' standard metal plasticity material model which is based on an incremental plasticity formulation employing associated flow assumptions in conjunction with a von Mises failure surface whose evolution in stress-space is governed by a simple isotropic hardening rule. In the present work, mild steel is considered; Fig. 3 displays a schematic representation of the uniaxial material response that is consistent with what is used in the present work.

2.2. Mesh

The models of the I-shaped cross-sections considered herein employ shell finite elements positioned along the middle surfaces on the cross-sectional constituent plate components in a fashion consistent with what is depicted in Fig. 4. The S4R nonlinear, finite strain, shell element from the ABAQUS element library is used exclusively. The S4R shell element is shear deformable and subsequently both reduced integration and the assumed strain method (MacNeal 1978) are employed to improve the overall thin-shell behavior of this element. A single integration point is used in this particular element hence stabilization of spurious zero energy modes is provided by ABAQUS. This element is selected for use in the parametric study based on its satisfactory performance in the verification work described in the papers by Thomas and Earls, and Greco and Earls (2003a,b).

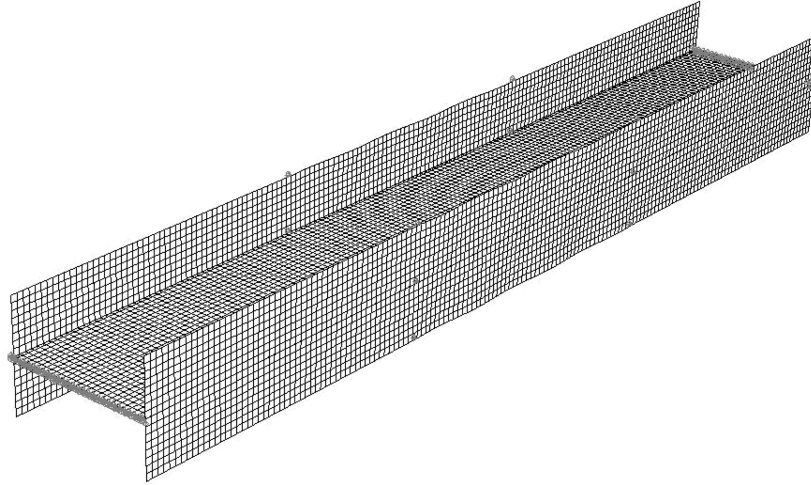


Fig. 4 Representative shell finite element mesh

2.3. Verification of modeling techniques

As it is that the nonlinear finite element modeling technique is the primary vehicle for the research program reported on herein, it is clearly of great importance to establish the accuracy of the modeling strategies used in the conduct of this work. A careful search of the experimental literature is undertaken in order that an appropriate research program might be identified for use as a test case for the current verification study.

The most appropriate study found in the literature centered on some work reported on at the University of Sydney (Rasmussen and Chick 1995). This experimental research program focused on the study of I-shaped members possessing slender cross-sectional profiles subjected to combined loading applied in a proportional fashion. As part of this Australian research, the extreme case of pure minor axis bending was considered and thus valuable experimental results were contained in this work vis-à-vis a verification study related to the present research.

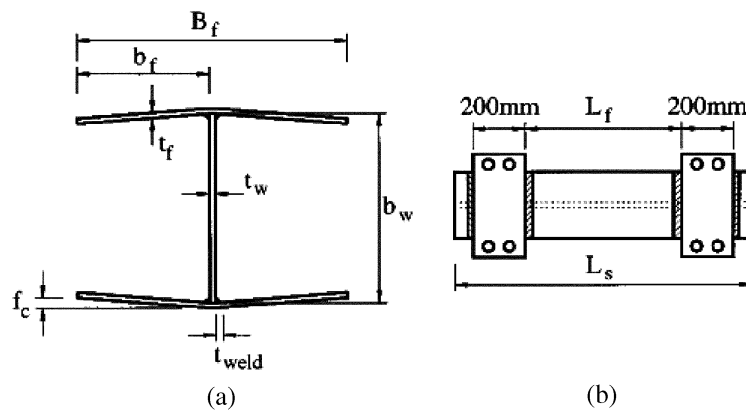


Fig. 5 Dimensions of experimental specimens tested by Rasmussen and Chick (1995)

Table 1 Measured specimen dimensions from Rasmussen and Chick (1995)

Specimen	Plate Number	E (GPa)	f_{yc} (MPa)	f_{yt} (MPa)	f_{ut} (MPa)
800-6	7	198	446	420	498
5800-5	4	200	466	431	509

Table 2 Measured material properties from Rasmussen and Chick (1995)

Specimen	L_s	L_f	t_f	t_w	b_w	B_f	f_c
	(mm)						
800-6	795.5	327	5.01	5.04	240	239	6
5800-5	5798	5175	4.98	5.02	241	240.5	5

Rasmussen and Chick (1995) focused on a single I-shaped cross-section whose nominal dimensions appear in Fig. 5. Using this single cross-section, three distinct study cases are considered through the variation of the member unbraced length. Specifically, short ($L_b = 800$ mm), medium ($L_b = 3500$ mm), and long ($L_b = 5800$ mm) members are treated in the work of Rasmussen and Chick (1995). As a focus of the current verification work, only the short and long cases are considered. In both of these members, the minimum specified yield strength of the steel is 350 MPa. Table 1 and Table 2 present the measured cross-sectional dimensions and experimentally determined steel mechanical response, respectively. It is noted that while it is that the reported mechanical response values from coupon testing given in Table 2 are in engineering units, these are converted to true stress and logarithmic strain values prior to importation into the finite element software package, ABAQUS. Tables 3 and 4 are used in conjunction with the schematic multi-linear uniaxial material response curve presented in Fig. 3 in order that the appropriate steel material representation is input into the verification model used in the current work.

Since the verification test case considered in this part of the study involves minor principal axis flexure of an I-shaped beam under the action of pure moment, bifurcation related response must be

Table 3 True stress and logarithmic strain values for specimen 800-6

σ_{nom} (MPa)	ϵ_{nom}	σ_{true} (MPa)	ϵ_{ln}^{pl}
420	0.0021	420.89	0
420	0.0167	427	0.014376
490.9	0.0577	519.22	0.053465
522.72	0.125	588.06	0.114813
522.72	0.2019	628.27	0.1807497

Table 4 True stress and logarithmic strain values for specimen for specimen 5800-5

σ_{nom} (MPa)	ϵ_{nom}	σ_{true} (MPa)	ϵ_{ln}^{pl}
431	0.0022	431.93	0
431	0.0231	440.95	0.0206099
510	0.0615	541.38	0.0570123
526.67	0.0885	573.26	0.081899
526.67	0.1462	603.64	0.1333936

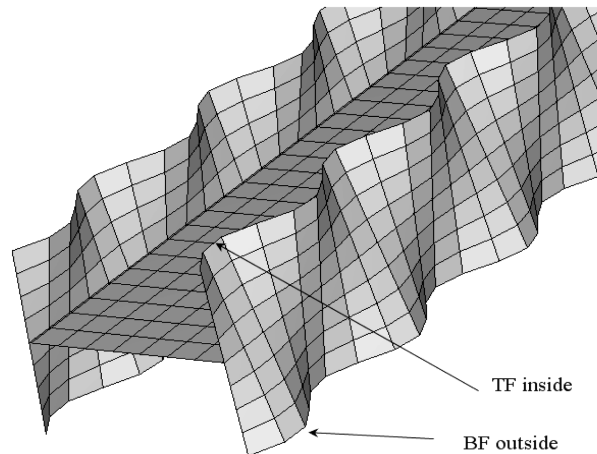


Fig. 6 Depiction of sinusoidally varying imperfection field

considered as a possible factor governing overall response. When applying the finite element method to bifurcation-type stability problems, it is oftentimes advisable to incorporate a reasonable imperfection field into the finite element model. The incorporation of the imperfection field is used to perturb the model from the condition of perfect geometry; failure to do this may result in the model artificially persisting in the perfect state throughout the loading history. The potential proximity of the finite element displacement solution to an initial perfect geometry arises since such a configuration is a mathematically admissible equilibrium state (even post bifurcation). However this configuration is meaningless physically since the slightest loading disturbance, or geometric imperfection, would render such an equilibrium state inaccessible to practical cases. As a means of guarding against any potentially physically aberrant response, a reasonable displacement-based imperfection field should be incorporated into finite element models whose response has the potential of being governed by bifurcation buckling. In such cases, it is not imperative that the precise governing buckling mode be used as an initial imperfection adopted at the start of the nonlinear solution. Rather, any imperfection field used need only possess elements of the dominant features that are contained in the governing mode.

In the present verification study, it is observed from linearized eigenvalue buckling analyses carried out with ABAQUS that the governing mode of instability in minor axis I-shaped members in pure bending involves localized buckling within the flange. In the current research, sinusoidally varying imperfections possessing a half wavelength of $B_f/2$, that is phase shifted by 180 degrees between opposite flange tips (see Fig. 6), is used in conjunction with a magnitude corresponding to the maximum allowable fabrication imperfection permitted by the American Welding Society (AWS D1.1:2000); a value of $B_f/100$ for the present work.

Employing the above specializations, the two constant moment minor axis flexural cases are reproduced in the computer in order that suitable structural response results can be generated and compared with the results from the experimental program of Rasmussen and Chick (1995). Plots comparing normalized moment and absolute rotation appear in Figs. 7 - 8. Based on these results, it appears that the present modeling techniques are sufficiently robust to undertake the outlined parametric study. Details of the modeling techniques germane to the current parametric study are treated below.

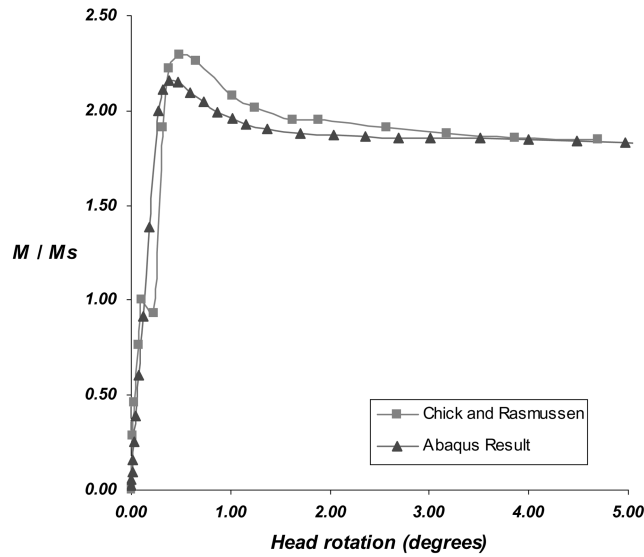


Fig. 7 Comparison of FE and experimental results: 800-6

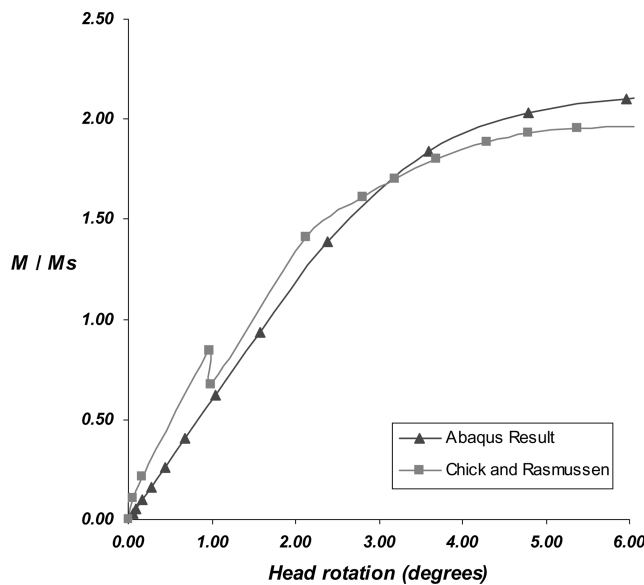


Fig. 8 Comparison of FE and experimental results: 5800-5

2.4. Model geometry for parametric study

This section reports on the results of a parametric study carried out using the same verified nonlinear finite element modeling approach discussed in the earlier sections of this paper. The same sinusoidally varying localized imperfection field of intensity $B_f / 100$ is used in this portion of the work. As a means of creating a constant moment region of investigation for this study, a three segment beam, acted on by two equally spaced concentrated transverse loads applied to the third points, is used to create a central

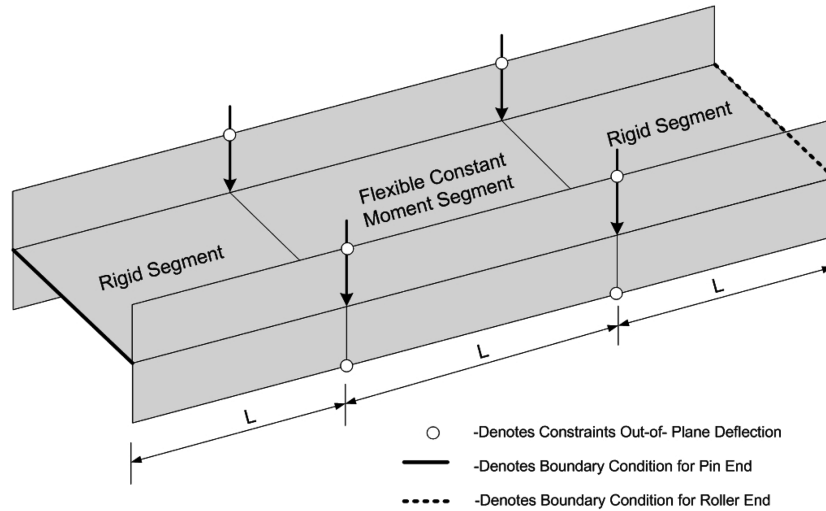


Fig. 9 Schematic of finite element representation used in parametric study

constant moment region possessing precisely the moment profile required by current specification writing bodies as the foundation case for provisions. The two end segments adjacent to the middle, constant moment region, are made to behave rigidly. A schematic depiction of the loading, geometry, and boundary conditions used in this work appears in Fig. 9.

Table 5 Parametric study naming convention

	$h/t_w = 60$	$h/t_w = 90$	$h/t_w = 120$
$F_y=345$ (MPa)	Group 1	Group 2	Group 3
$F_y=414$ (MPa)	Group 4	NA	NA
$F_y=483$ (MPa)	Group 5	NA	NA

Table 6 Group 1 results

		$F_y=345$ (MPa)			$h/t_w=60$		
		B_f / d					
		0.4	0.5	0.6	0.7	0.8	0.9
L / B_f	2	9.5	8.5	8.5	8	8	8
	3	9.5	8.5	8.5	8	8	8
	4	10	9	8.5	8.5	8	8
	5	na	na	9	8.5	8	8
	6	11.5	10	9	8.5	8.5	8.5
	7	na	10	9	9	8.5	8.5
	8	na	10	9.5	9	8.5	8.5
	9	na	10.5	9.5	9	8.5	8.5

Table 7 Group 2 results

		$F_y=345$ (MPa)				$h/t_w=90$	
		B_f/d					
		0.4	0.5	0.6	0.7	0.8	0.9
L/B_f	2	8.5	8	8	8	7.5	7.5
	3	8.5	8	8	8	7.5	7.5
	4	9	8.5	8	8	7.5	7.5
	5	9	8.5	8	8	8	7.5
	6	9	8.5	8	8	8	7.5
	7	9	8.5	8	8	8	7.5
	8	9.5	8.5	8	8	8	7.5
	9	9.5	8.5	8	8	8	7.5

Table 8 Group 3 results

		$F_y=345$ (MPa)				$h/t_w=120$	
		B_f/d					
		0.4	0.5	0.6	0.7	0.8	0.9
L/B_f	2	8.5	8	8	7.5	7	6.5
	3	na	8	na	7.5	na	6.5
	4	8.5	8	8	7.5	7	6.5
	5	8.5	8	8	7.5	7	7
	6	8.5	8	8	na	7	7
	7	8.5	8	8	8	7	7
	8	8.5	8	8	8	na	na
	9	8.5	8.5	8	8	7.5	7

Table 9 Group 4 results

		$F_y=414$ (MPa)				$h/t_w=60$	
		B_f/d					
		0.4	0.5	0.6	0.7	0.8	0.9
L/B_f	2	8	7.5	7.5	7.5	7.5	7.5
	3	8	7.5	7.5	7.5	7.5	7.5
	4	8.5	8	7.5	7.5	7.5	7.5
	5	9	8	8	7.5	7.5	7.5
	6	10	8.5	8	8	7.5	7.5
	7	10	9	8.5	8	7.5	7.5
	8	na	9	8.5	8	8	7.5
	9	na	9	8.5	8.5	8	8

Table 10 Group 5 results

		$F_y=483$ (MPa)			$h/t_w=60$		
		B_f/d					
		0.4	0.5	0.6	0.7	0.8	0.9
L/b_f	2	7.5	7	7	7	7	7
	3	7.5	7	7	7	7	7
	4	7.5	7.5	7	7	7	7
	5	8	7.5	7.5	7	7	7
	6	8.5	8	7.5	7.5	7	7
	7	9	8	8	7.5	7.5	7.5
	8	9	8.5	8	7.5	7.5	7.5
	9	9	na	8	7.5	7.5	7.5

3. Description of parametric study and discussion of approach

The present parametric investigation considers the variation of five physical quantities: cross-sectional aspect ratio (B_f/d); unbraced length-to-cross-sectional depth ratio (L_b/b_f); web slenderness ratio, (h/t_w); flange slenderness ratio, ($B_f/2t_f$), and steel yield strength (F_y). The individual parameters are varied within the context of five groupings of a series of given quantities as defined in Tables 5 and listed in detail in Tables 6, 7, 8, 9, and 10. When arriving at individual plate slenderness limits for compact flange response, the ratio $B_f/2t_f$ is varied for a fixed combination of the other four parameters until compact response is achieved (see Fig. 10 for a schematic depiction of this approach).

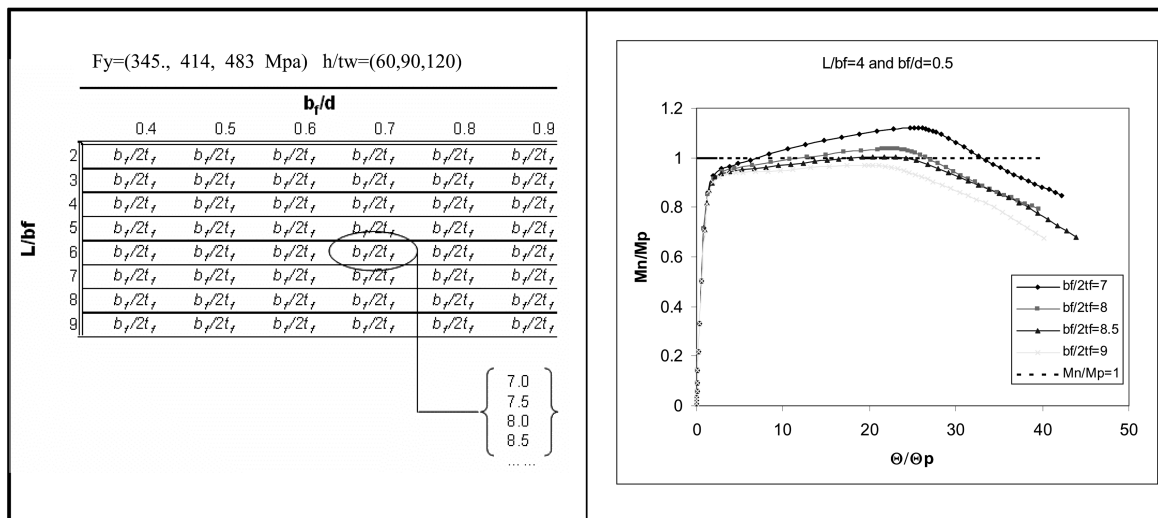


Fig. 10 Depiction of approach taken in arriving at compactness results (note: b_f refers to the complete flange width in this figure)

4. Results

More than 40 discrete parametric data points are obtained from an analysis space of more than 200 individual runs. The 40 discrete parametric points are tabulated in Tables 6, 7, 8, 9, and 10. In addition, some representative trend lines are plotted in Fig. 11.

The described data set is subsequently used to make observations and generalizations regarding the behavior of I-shaped cross-sections subjected to constant minor axis flexure.

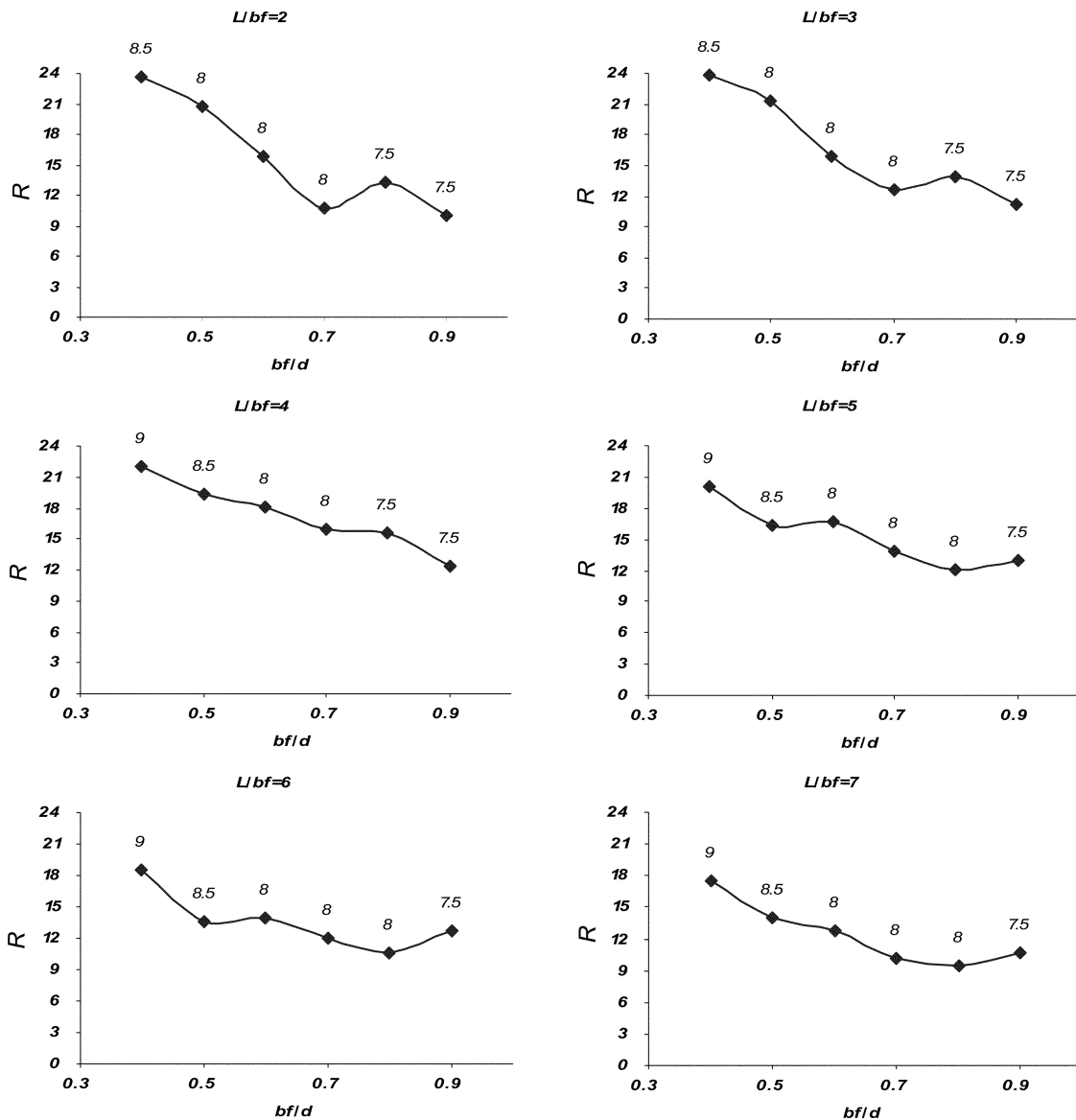


Fig. 11 Representative trends in results from parametric study: rotation capacity vs. aspect ratio (note: b_f refers to the complete flange width in this figure)

5. Discussion of results

As the parameters of the study are varied, certain trends in behavior become clear. The current section endeavors to describe the observed differences as well as to describe possible mechanisms that may explain the observed response and thus lend additional insight into the problem of minor axis compactness.

One discussion point that conspicuously presents itself is related to the applicability of exiting specification recommendations, for major axis flexural flange compactness, to the case of minor axis flexure. While it is believed that the foregoing practice is conservative, this may not actually be the case. Based on the results presented herein for the three steel grades considered, it appears to be un-conservative to apply the major axis provisions to the case of minor axis flexure. For the case of steel with a minimum specified yield stress of 345 MPa, the US specification requires that for compactness, the ratio $B_f / 2t_f$ may not exceed 9.2. However, the results presented herein clearly indicate that the maximum permissible plate ratio $B_f / 2t_f$ may be as low as 6.5 (depending on web slenderness ratio, h / t_w , and cross-sectional aspect ratio, B_f / d). Similar results hold for the cases with steel having yield stresses of 414 MPa and 483 MPa.

5.1. Effect of steel yield strength on flange compactness limit

Based on the compactness results gleaned from the finite element modeling results obtained using steel possessing yield strengths of 345 MPa, 414 MPa, and 483 MPa, certain trends in cross-sectional compactness arise. As the yield strength increases from 345 MPa to 483 MPa, the maximum permissible cross-sectional plate slenderness ratio decreases by as much as 25%. Meaning that as steel strength increases, a significantly more strict compactness limit must be enforced as compared with cross-sections made from lower strength steels. It is noted that this sensitivity to yield stress is somewhat greater than what the US specification predicts (15% decrease in maximum permissible limiting plate slenderness resulting from the noted 138MPa steel strength increase – all other parameters held constant). However, it is noted that in cases where the cross-section possesses a large cross-sectional aspect ratio, B_f / d , (approximately 0.9) the diminution of the maximum permissible flange slenderness resulting from the increasing steel strength is much more consistent with current specification predictions; although overall magnitude of the slenderness limit predicted by the specifications is still un-conservative.

5.2. Effect of web slenderness on flange compactness limit

A clear parameter influencing the maximum permissible flange slenderness limit is the cross-sectional web slenderness, h / t_w . Using the web compactness limit from the US specification (in conjunction with a steel yield strength of 345 MPa) for the case of major axis flexure as some reasonable point of departure for the present parametric study, a web slenderness limit of 90 is considered as some baseline for variation. As part of the current research effort, a variation of +/- 30% of this value (i.e., $h / t_w = 60, 90, \text{ and } 120$) is considered in the following discussion. As web slenderness, h / t_w , increases, the maximum permissible flange slenderness required for compact behavior decreases (in some cases by as much as 25% as h / t_w increases by 100%).

5.3. Effect of cross-sectional aspect ratio on flange compactness limit

It is interesting to note that the ratio of cross-sectional flange width to cross-sectional depth ratio, B_f/d (aspect ratio), has a pronounced influence on the limiting flange slenderness required for compact response. In general, as the aspect ratio increases (from 0.4 to 0.9), decreases as large as 25% are observed to occur in the limiting flange slenderness. This would indicate that, as an isolated parameter, cross-sectional aspect ratio is at least as important as web slenderness in affecting limiting flange slenderness requirements for compact response in minor axis flexure. However, it is pointed out that as the span-to-depth ratio approaches seven (7), the fluctuation in flange compactness as a function of cross-sectional aspect ratio all but disappears.

5.4. Effect of span-to-depth ratio on flange compactness limit

In the present research, a series of different span-to-depth ratios, L_b/B_f are considered; ranging from 2 to 9. Based on the authors experience in modeling and experimental testing, beams whose span-to-depth ratio is greater than or equal to 7 tend to behave well; vis-à-vis Bernoulli-Euler beam theory. Those beams whose span-to-depth ratios are less than 7 tend to exhibit significant effects of internal shear. This fact is pointed out since it is noted that as the span-to-depth ratio increases in the test population considered in the current research, increases in concomitant flange slenderness limits accompany this growth; increasing by as much as 17% in the most extreme instance (all other parameters held constant).

5.5. Effect of web-restraint on flange compactness limit

Based on the foregoing, it seems that the major factors influencing minor axis flange compactness are web slenderness and cross-sectional aspect ratio. However, a closer examination of the results hints at a mechanical basis for this: the effect of web-restraint on the inelastic flange buckling. In arriving at this conjecture, it is observed that at low span-to-depth ratios, the reduction in the flange compactness limit, as a function of cross-sectional aspect ratio, is greatest. In addition, at high span-to-depth ratios, the flange slenderness limit for compactness is quite steady across different cross-sectional aspect ratios, and this steadiness occurs in conjunction with the largest observed permissible values for the flange slenderness.

One may use the foregoing, in conjunction with the observation that flange compactness limits are somewhat insensitive to changes in span-to-depth ratio, to shed light on an obvious limitation in the modeling: the presence of rigid ends in the model. It might have been surmised that the rigid ends would provide an artificially high restraint against local buckling and thus improve structural ductility; allowing for more liberal flange compactness limits. Such a restraining effect ought to be most pronounced as the span lengths decrease and the rigid ends subsequently move closer together. In actuality, the opposite trend is observed and the most liberal minor axis flange compactness limits occur at the larger span-to-depth ratios for the beam in question. So the question remains; if some restraint of the flanges is leading to increases in compactness limits then where is the restraint coming from? The hypothesis is that the restraint is coming from the web. Based on the research results, it is noted that as the web slenderness increases, it is easier for the flange to buckle locally. This may be ascribed to the reduced flexural rigidity in the web as its slenderness is increased. It is further pointed out that this web restraint effect appears to be more pronounced in cases wherein the member in minor axis flexure is

permitted to act like a beam (i.e., when span-to-depth ratios are greater than or equal to 7). At lower span-to-depth ratios, the effects of shear complicate the observed response and thus make it difficult to find a mechanistic basis for observed differences in flange compactness.

5.6. Comparison with Eq. (6)

The approach taken in deriving Eq. (6) in the introduction of the current paper is philosophically consistent with what the US Specification (AISC 1999) has done for the case of flange outstands subjected to compression due to major axis flexure. Applying the one third difference between the plate buckling coefficients, that is subsequently added to the lower bound value, produces a plate slenderness limit, for compactness in 345 MPa flanges, of 10.2; a value far in excess of what is observed to be a safe limit from the current finite element modeling results. A more appropriate use of an Eq. (6) approach might be to preserve the plate buckling coefficient associated with the pinned supported plate edge (0.57) wherein a more reasonable value of 7.9 is arrived at for a flange slenderness limit, $B_f / 2t_f$, as required for compact cross-sectional response for use in conjunction with 345 MPa steel. Limiting flange slenderness values of 7.3 and 6.7 are also obtained from this approach in the case of steel with yield strengths of 414 MPa and 483 MPa, respectively. While it is that such an approach may be on the conservative side for the parametric space explored, the method is flawed in a phenomenological sense since it tacitly denies the relevance of edge restraint which has clearly been shown to be of importance to this problem. However, as a simple and easily understood means for prescribing minor axis flange compactness limits, it may be of some use despite these obvious limitations.

6. Conclusions

For the case of I-shaped beams bent about the minor principal centroidal axis, it appears to unconservative to apply limiting plate slenderness ratios for the major principal axis flexural case when significant structural ductility is sought. Indeed, proper consideration of reserve capacity during inelastic buckling of constituent plate buckling elements used in the flanges must properly consider the important effects of rotational edge restraint afforded by the web along the flange-web junction.

As a crude but useful measure, one may deny the importance of this edge restraint and rely on a simple, but conservative plate slenderness limit that is not too philosophically different from the equations employed in the major axis flexural case and thus easily incorporated into existing specification formats.

References

- ABAQUS (2003), *ABAQUS Theory Manual*, Hibbit, Karlsson & Sorensen, Inc., Pawtucket, Rhode Island, USA.
- AISC (1999), *Load and Resistance Factor Design Specification for Structural Steel Buildings, 3rd Ed.*, American Institute of Steel Construction Inc., Chicago, Illinois.
- ASCE (1971), *Plastic Design in Steel, A Guide and Commentary*, American Society of Civil Engineers, New York, New York, p. 80.
- AWS D1.1 (2000), *American Welding Society – Structural Welding Code*, U.S.A.
- Bradford, M. A. (1994), “Elastic local buckling of flange outstands with idealized edge restraint”, *Eng. Struct.*,

- 14, 242-248.
- Bradford, M. A. and Azhari, M. (1994), "Local buckling of I-sections bent about the minor axis", *J. Construct. Steel Res.*, **31**, 73-89.
- Galambos, T. V. (1998), *Guide to Stability Design Criteria for Metal Structures*, Fifth Edition, John Wiley & Sons, Inc., New York, New York.
- Greco, N. and Earls, C. J. (2003b), "Structural ductility in hybrid high performance steel beams", *J. Struct. Eng.*, ASCE, **129**(12), 1584-1595.
- Haaijer, G. and Thurlimann, B. (1958), "On inelastic buckling in steel", *J. Eng. Mech. Div., Proc. of the American Society of Civil Engineers*, Paper 1581, EM 2, April, pp. 1581-1 to 1581-48.
- MacNeal, R. H. (1978), "A simple quadrilateral shell element", *Comput. Struct.* Pergamon Press Ltd., Great Britain, **8**, 175-183.
- Rasmussen, K. J. R. and Chick, C. G. (1995), "Tests of thin walled I-section in combined compression and minor axis bending – Part II – Proportional Loading Tests", University of Sydney – School of Civil and Mining Engineering Research Report No. R717.
- Thomas, S. and Earls, C. J. (2003a), "Cross sectional compactness and bracing requirements for HPS483W girders", *J. Struct. Eng.*, ASCE, **129**(12), 1569-1583.

Notation

B_f	: complete flange width
b_f	: flange outstand width ($B_f / 2$ except where noted)
b	: plate width dimension
t	: plate thickness
t_f	: flange thickness
t_w	: web thickness
E	: elastic modulus
F_y, σ_y	: steel yield stress
F_u, σ_u	: steel ultimate stress
L, L_b	: unbraced beam length
M	: applied bending moment
M_s	: fully plastic cross-sectional capacity
R	: cross-sectional rotation capacity
b_w, h, d	: web depth
λ_c	: plate slenderness ratio
ν	: poisson's ratio
ε	: strain

CC